Earth and Planetary Science Letters 287 (2009) 194–204

Contents lists available at ScienceDirect

Earth and Planetary Science Letters

journal homepage: www.elsevier.com/locate/epsl

Ultra-depleted melts from Kamchatkan ophiolites: Evidence for the interaction of the Hawaiian plume with an oceanic spreading center in the Cretaceous?

Maxim Portnyagin [a,b,*], Kaj Hoernle [a], Dmitri Savelyev [c]

[a] Leibniz Institute of Marine Sciences, IFM-GEOMAR, Wischhofstrasse 1-3, 24148 Kiel, Germany
[b] V.I.Vernadsky Institute of Geochemistry and Analytical Chemistry, Kosigin str. 19, 119991 Moscow, Russia
[c] Institute of Volcanology and Seismology, Piip Boulevard 9, Petropavlovsk-Kamchatsky, 683006, Russia

ARTICLE INFO

Article history:
Received 28 May 2009
Received in revised form 22 July 2009
Accepted 30 July 2009
Available online 13 September 2009

Editor: R.W. Carlson

Keywords:
Kamchatka
ophiolite
ultra-depleted melts
melt inclusion
spinel
plume–ridge interaction
Hawaiian hotspot

ABSTRACT

We report new data on the major and trace element composition of melt inclusions in spinel phenocrysts (Mg# = 0.7–0.8, Cr/(Cr + Al) = 0.32–0.52, TiO_2 = 0.06–0.60 wt.%) from Cretaceous MORB-like basalt (La/Yb = 0.94, Th/Nb = 0.055, Th/La = 0.041) in the Kamchatsky Mys ophiolites (Eastern Kamchatka). The melt inclusions preserved primitive melts (Mg# up to 0.72), which are remarkably depleted in incompatible trace elements compared to common MORBs. Numerous ultra-depleted inclusions from the studied sample have extraordinarily low Na_2O (0.20–0.67 wt.%), TiO_2 (0.16–0.5 wt.%), K (1.5–25 ppm), La (0.015–0.040 ppm), Zr (0.9–2 ppm), B (0.01–0.03 ppm), Ti/Zr = 300–1074, La/Yb = 0.008–0.075 and represent the most depleted melts known until now. The ultra-depleted melts from the Kamchatkan ophiolites are only comparable to a single melt inclusion from MORB of 9°N Mid-Atlantic Ridge [Sobolev and Shimizu, Nature 363 (1993) 151–154] yet have higher FeO, CaO, heavy rare-earth element (Dy, Er, Yb) contents and lower Na_2O and SiO_2. These melts, possibly the last melt fractions produced in an upwelling mantle column, could represent the highest degrees (up to ~20%) of near-fractional melting of mantle with $T_p \geq 1400$ °C, which started melting at ~75 km depth and continued to shallow depths of ~20 km. The presence of melts ranging in composition from ultra-depleted to compositions similar to Mauna Loa Volcano, Hawaii, high potential mantle temperature and association with rocks akin the Cretaceous Hawaiian tholeiites suggest that the trace element depleted melts preserved in spinel phenocrysts could have originated from extensive melting of a depleted component intrinsic to the Hawaiian plume or ambient upper mantle entrained and heated up at the plume margins.

1. Introduction

Ophiolites, fragments of oceanic lithosphere occasionally preserved on land at active continental margins, provide a unique opportunity to obtain information about the composition and origin of older, than preserved on the ocean floor, oceanic crust, which has generally been subducted into the mantle (Hauff et al., 2000; Pearce, 2008). Of the numerous ophiolites in the circum Pacific, Kamchatsky Mys ophiolites in Eastern Kamchatka (Fig. 1A) have received considerable attention recently, due to their peculiar tectonic setting at the junction of Kamchatka and Aleutian Arcs, their Early to middle Cretaceous age and the geochemical diversity of ophiolitic sequence (Fedorchuk, 1992; Khotin and Shapiro, 2006; Portnyagin et al., 2008; Portnyagin et al., 2005b; Saveliev, 2003).

A study of the Kamchatsky Mys ophiolites can provide insights into the poorly known Cretaceous magmatic history of the NW Pacific. An intriguing finding from recent detailed geochemical studies of the ophiolites was the discovery of volcanic rocks with Hawaiian trace element and isotope signature, consistent with preservation of older (Early to middle Cretaceous) products of the Hawaiian hotspot through accretion to the Kamchatkan forearc (Portnyagin et al., 2008). An important question arising from these results concerns the genetic relationships among the different geochemical groups of basalts in the ophiolites. Geochemically diverse ophiolitic rocks could either have been tectonically juxtaposed during collision (Fedorchuk, 1992) or have formed in a close temporal and spatial tectonic framework, possibly influenced by the Hawaiian hotspot (Portnyagin et al., 2008; Portnyagin et al., 2005b; Saveliev, 2003).

Here we report new major and trace element data from homogenized melt inclusions in spinel from the Kamchatsky Mys ophiolites. These inclusions are moderately to ultra-depleted in incompatible trace elements, extending to the most depleted compositions reported thus far. These ultra-depleted melts can represent the last fractions of melt originated at shallow depths by near-fractional melting of an upwelling mantle column. The presence of melts ranging in composition from ultra-depleted to Hawaiian-like, elevated potential mantle temperature (≥1400 °C) and the association with rocks akin to Cretaceous Hawaiian

* Corresponding author. Leibniz Institute of Marine Sciences, IFM-GEOMAR, Wischhofstrasse 1-3, 24148 Kiel, Germany.
E-mail address: mportnyagin@ifm-geomar.de (M. Portnyagin).

0012-821X/$ – see front matter © 2009 Elsevier B.V. All rights reserved.
doi:10.1016/j.epsl.2009.07.042

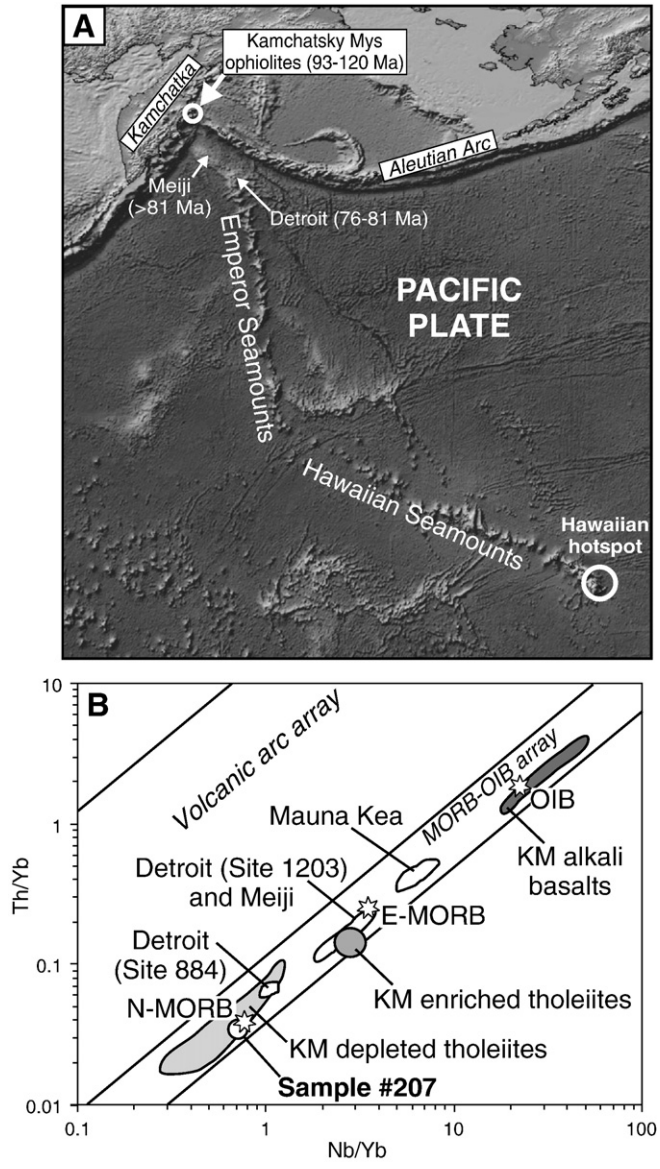

Fig. 1. Overview map of the NW Pacific and major compositional features of the Kamchatsky Mys ophiolites in the Eastern Kamchatka: (A) Location of the Kamchatsky Mys ophiolite massif in eastern Kamchatka, adjacent to the end of the Hawaiian–Emperor Seamount chain; (B) Composition of volcanic rocks from the Kamchatsky Mys (KM) ophiolites. Compositional fields of alkali basalts, depleted and enriched tholeiites are shown after Portnyagin et al. (2008). Sample #207 studied here belongs to the group of depleted N-MORB-like tholeiites. Compositions of N-MORB, E-MORB and OIB (Sun and McDonough, 1989), Cretaceous shield-stage tholeiites from Meiji and Detroit Seamounts (Huang et al., 2005; Keller et al., 2000; Regelous et al., 2003), Mauna Kea tholeiites (Hofmann and Jochum, 1996; Huang and Frey, 2003) are shown for comparison.

tholeiites are consistent with the origin of the ultra-depleted melts at an oceanic spreading center interacting with the Hawaiian hotspot in the Cretaceous.

2. Kamchatsky Mys ophiolites and studied samples

The ophiolite complex is located in the southwestern part of the Kamchatsky Mys Peninsula (Eastern Kamchatka) (Fig. 1A) and consists of a deformed association of ultramafic rocks, gabbros, dolerites, basalts and sediments (e.g. Fedorchuk, 1992; Khotin and Shapiro, 2006). The ophiolites are interpreted to be a part of an accretionary wedge of the paleo-Kronotsky Arc formed during the Late Cretaceous–Eocene at 36–45°N latitude (Khotin and Shapiro, 2006; Lander and Shapiro, 2007), which is now a constituent of the Kamchatka forearc. Volcanic rocks in the ophiolites occur in the ~1.5 km thick Smagino association together with hyaloclastites and intercalated red jasper and pink pelitomorphic limestone, consistently dated paleontologically as Albian–Cenomanian (112–93 m.y.; Khotin and Shapiro, 2006 and references therein). Volcanic rocks of the Smagino association, occurring in tectonically separated blocks, range from trace element depleted to slightly enriched mid-ocean-ridge-like basalts (MORB-like) to alkali basalts (Fig. 1B). Several studies have proposed that the ophiolite assemblage originated through the interaction of a hotspot (plume), possibly the Hawaiian, with a mid-ocean ridge (Khotin and Shapiro, 2006; Portnyagin et al., 2005b; Saveliev, 2003). Recently published bulk rock and melt inclusion data on a group of enriched tholeiites from the ophiolites provide strong support for a genetic link to the Hawaiian hotspot (Portnyagin et al., 2008).

The present study was focused on MORB-like sample (#207, N56°07′05″ E163°4′29″) collected from a block in a serpentinite mélange in the ophiolite complex, which hosts abundant and unusually Ti-poor spinel phenocrysts (Portnyagin et al., 2005b). The rock is an altered olivine–plagioclase–phyric basalt with high concentrations of Cr (749 ppm) and Ni (219 ppm), low concentrations of immobile (in low-temperature hydrothermal fluids) incompatible (during mantle melting) trace elements (La = 2.5 ppm, Th = 0.10 ppm, Nb = 1.8 ppm low ratios of more to less incompatible elements (e.g. La/Yb = 0.94, Th/Nb = 0.055 and Th/La = 0.041) and radiogenic initial $^{143}Nd/^{144}Nd$ (0.51310 at 100 My) and thus has similar chemical characteristics to MORB (Fig. 1B; Table 1). Since the whole rock and primary silicate minerals (plagioclase and olivine) did not survive the low-temperature alteration in the studied rocks, we focused our study aimed at deciphering the composition of parental melts on accessory spinel. Spinel not only resists alteration well but is the first liquidus phase, together with olivine, of mantle-derived magmas and thus can provide information about primitive magma composition (Dick and Bullen, 1984; Kamenetsky et al., 2001).

Octahedral chromium spinel phenocrysts up to 0.5 mm in size and inclusions in altered olivine compose ~1% of the rock. The spinels are Mg-rich (Mg# = 0.70–0.80 where Mg# is molar $Mg/(Mg+Fe^{2+})$), moderately Cr-rich (molar $Cr/(Cr+Al) = 0.32–0.52$), highly reduced (molar $Fe^{3+}/(Fe^{3+}+Al+Cr) = 0.03–0.06$) and extend to very low-Ti ($TiO_2 = 0.06–0.60$ wt.%) compared to spinel in MORB (Kamenetsky et al., 2001) and in other MORB-like samples from the Kamchatsky Mys (KM) ophiolite massif (Portnyagin et al., 2008; Portnyagin et al., 2005b) (Fig. 2). Many spinel crystals contained partially crystallized melt inclusions.

3. Methods

Spinel crystals were separated under a microscope from crushed 0.25–0.5 mm fraction of the whole rock. Melt inclusions are regularly distributed throughout the host crystals and consist of an assemblage of secondary ("daughter") phases, Ca pyroxene, high-Al andesitic glass, shrinkage gas bubble and often small sulfide globules, which crystallized from trapped melt at decreasing ambient temperature (Fig. 3A). Compositions of the daughter phases were reported in Portnyagin et al. (2005b). To eliminate the effects of post-entrapment crystallization inside inclusions, spinel grains were heated to 1250 °C and quenched. Experimental studies were performed at IFM-GEOMAR (Kiel, Germany) using a heating stage for micro-thermometric studies (Sobolev and Slutskii, 1984). The heating stage operated at 0.1 MPa pressure of ultra-pure helium. Temperature was controlled with Pt–$PtRh_{10}$ thermocouple calibrated every run against the melting-point of pure gold. Duration of runs was ~10 min. Rapid quenching (200 °C/s) was achieved by simultaneously switching off the electric supply on the heater and opening gas flow through the experimental chamber. After each experiment, spinels were gradually polished to expose melt inclusions. Optical investigations confirmed that most inclusions were

Table 1
Major and trace element composition of host rock, melt inclusions and their host spinels.

N	Host rock	Melt inclusions															
Sample #	207	2a	6a	9m	14a	45a	3a	44a	10	32	5	X	SP1a	SP7a	SP8b	SP8c	SP8a
Experiment[a]		h	h	h	h	h	h	h	h	h	h	h	u	u	u	u	u-alt
Diameter (μm)		48	40	108	60	60	50	50	150	70	60	50	70	80	30	30	30
SiO_2	45.79	51.74	50.89	50.58	49.98	51.34	50.32	50.85	50.76	51.78	50.59	50.58	50.57	52.08	51.17	51.52	48.25
TiO_2	1.18	0.34	0.27	0.16	0.33	0.50	0.54	0.50	0.47	0.39	0.60	0.72	0.22	0.50	0.53	0.52	0.57
Al_2O_3	15.79	17.02	15.62	16.81	15.45	15.85	15.67	15.85	15.53	16.84	15.87	15.01	19.48	19.66	18.68	18.76	19.97
FeO	10.01	8.02	8.38	7.86	8.59	8.37	7.68	8.39	7.34	6.92	8.34	7.99	6.30	7.02	6.68	6.96	6.23
MnO	0.23	0.15	0.11	0.14	0.12	0.06	0.16	0.12	0.080	0.12	0.11	0.13	0.08	0.13	0.16	0.15	0.23
MgO	5.84	7.17	10.21	8.79	9.96	10.45	10.47	10.95	10.10	9.02	9.47	11.29	8.32	8.87	8.05	7.45	4.6
CaO	9.57	14.81	14.18	14.91	14.06	13.79	13.67	13.84	14.02	13.87	13.96	13.85	12.61	10.39	13.12	10.72	8.72
Na_2O	2.85	0.38	0.28	0.41	0.32	0.41	0.76	0.32	0.67	1.13	0.51	0.61	1.46	2.13	2.11	2.25	2.23
K_2O	2.18	0.004	0.006	0.016	0.004	0.009	0.015	0.011	0.020	0.026	0.002	0.039	0.034	0.008	0.046	0.02	3.62
P_2O_5	0.13	0.035	0.009	0.033	0.018	0.006	0.023	0.028	0.028	0.067	0.021	0.060	0.038	0.020	0.024	0.03	0.01
S	na	0.084	0.091	0.097	0.093	0.125	0.106	0.126	0.086	0.123	0.080	0.109	0.070	na	na	na	na
Cl	na	0.011	0.000	0.002	0.006	0.011	0.011	0.006	0.005	0.025	0.005	0.006	0.011	na	na	na	na
Cr_2O_3	0.08	0.47	0.53	0.21	0.80	0.39	0.38	0.50	0.30	0.28	0.43	0.41	0.98	0.42	0.67	1.3	1.15
Total	93.65	100.23	100.57	100.03	99.72	101.31	99.80	101.49	99.41	100.59	99.98	100.80	100.17	101.23	101.24	99.67	95.58
Melt Mg#	0.51	0.61	0.68	0.67	0.67	0.69	0.71	0.70	0.71	0.70	0.67	0.72	0.70	0.69	0.68	0.66	0.57
Cr[b]		10,020	39,733	260	10,667	1246	11,000	3848	3151	452	7613	1989	11,300	483	29,482	23,526	28,686
X_{sp} (wt.%)[c]		3.6	13.7	0.1	3.6	0.4	4.0	1.3	1.1	0.2	2.7	0.7	4.1	0.2	10.8	8.6	10.5
Li	6.9	2.0	3.0	2.1	2.5	2.6	2.8	2.9	2.0	2.4	2.5	3.2	3.8	3.9	4.5	4.5	4.0
Be	na	0.007	0.029	0.001	0.025	0.051	0.050	0.049	0.035	0.031	0.044	0.059	0.039	0.056	0.061	0.060	0.45
B	na	0.033	0.011	0.024	0.021	0.017	0.023	0.031	0.048	0.13	0.12	0.10	1.27	0.52	0.30	0.13	20
K	18,094	12.05	1.7	6.1	3.4	8.9	8.2	36	43	133	73.11	173	427	114	523	74	52,016
Ti	7080	2621	2201	1251	2149	3011	3394	3048	2506	2150	3489	3739	1871	3308	3656	3582	6073
V[d]	*312*	*393*	*571*	*320*	*392*	*268*	*311*	*280*	*271*	*181*	*313*	*270*	*247*	*211*	*460*	*408*	*578*
Sr	426	4.1	1.2	1.7	2.6	1.5	5.5	15.3	9.0	31.3	28.1	35.1	69.0	25.8	75.7	53.5	818
Y	29	12.7	11.8	8.7	11.6	15.6	17.5	15.3	11.4	12.5	17.1	18.1	11.0	15.5	17.6	16.5	24.1
Zr	55	4.5	1.9	0.87	2.3	6.1	10.9	5.3	6.7	14.9	8.2	10.2	13.9	13.7	22.3	13.8	49.3
Ba	277	0.042	0.058	0.105	0.019	0.034	0.032	0.54	1.1	2.9	0.16	2.7	7.0	2.4	9.4	1.9	383
La	2.5	0.049	0.020	0.017	0.015	0.017	0.040	0.13	0.14	0.529	0.37	0.528	0.900	0.264	1.290	0.275	1.07
Ce	6.39	0.35	0.039	0.097	0.098	0.084	0.18	0.43	0.49	1.80	1.24	1.25	2.73	1.06	4.03	0.92	3.01
Nd	6.46	0.27	0.18	0.20	0.21	0.16	0.32	0.43	0.82	2.04	0.56	0.56	2.32	1.77	4.01	1.65	4.56
Sm	2.42	0.24	0.29	0.25	0.17	0.30	0.50	0.23	0.54	1.19	0.25	0.37	0.97	1.11	1.72	1.02	1.43
Eu	0.94	0.14	0.16	0.12	0.10	0.13	0.25	0.10	0.25	0.39	0.15	0.22	0.40	0.45	0.73	0.37	0.35
Gd	3.42	0.83	0.79	0.51	0.62	0.94	1.48	0.86	0.88	1.33	1.01	1.01	1.37	2.01	2.62	2.86	2.73
Dy	4.46	1.62	1.36	1.16	1.62	2.32	2.69	2.26	1.68	2.02	2.53	2.77	1.72	2.48	2.79	2.94	3.70
Er	2.69	1.22	1.41	0.92	1.35	1.98	1.85	1.97	1.39	1.35	1.85	2.10	1.08	1.70	1.70	2.04	2.88
Yb	2.67	1.18	1.64	1.09	1.59	1.84	1.74	2.06	1.54	1.44	1.75	2.16	1.13	1.73	1.90	2.39	2.31
Th	0.10	bdl	0.031	bdl	bdl	bdl	0.005	0.019	0.008	0.037	0.008	0.023	0.043	0.006	0.034	0.017	0.061
U	0.21	bdl	0.022	bdl	0.010	bdl	0.017	0.017	bdl	0.023	0.014	0.015	0.033	0.021	0.044	bdl	0.10
Host spinel																	
SiO_2		0.08	0.10	0.08	0.08	0.08	0.10	0.10	0.08	0.08	0.10	0.09	0.07	0.09	0.05	0.05	0.05
TiO_2		0.14	0.13	0.07	0.14	0.19	0.22	0.20	0.19	0.16	0.20	0.23	0.12	0.19	0.18	0.18	0.18
Al_2O_3		28.18	26.81	33.75	26.55	27.20	29.78	28.04	26.73	29.27	28.22	28.99	27.93	31.62	31.11	31.11	31.11
Cr_2O_3		40.91	42.39	34.55	42.89	43.10	39.86	42.24	42.74	41.15	41.58	40.74	42.21	36.49	37.69	37.69	37.69
Fe_2O_3[e]		2.88	3.09	3.13	3.23	33.20	22.61	33.11	22.87	22.68	22.60	22.80	22.19	33.43	22.84	22.84	22.84
FeO		11.28	9.97	10.95	10.22	10.30	10.51	10.33	11.36	10.72	10.57	10.38	11.51	9.75	10.38	10.38	10.38
MnO		0.14	0.14	0.10	0.09	0.15	0.16	0.15	0.16	0.16	0.13	0.17	0.17	0.15	0.15	0.15	0.15
MgO		16.51	17.11	17.19	17.04	17.33	17.27	17.44	16.39	17.26	17.09	17.30	16.39	17.77	17.29	17.29	17.29
NiO		0.12	0.20	0.18	0.22	0.20	0.20	0.18	0.16	0.14	0.17	0.22	0.13	0.16	0.18	0.18	0.18
Total		100.24	99.93	100.01	100.47	101.75	100.70	101.78	100.68	101.63	100.68	100.93	100.72	99.65	99.87	99.87	99.87
Spinel Mg#		0.72	0.75	0.74	0.75	0.75	0.75	0.75	0.72	0.74	0.74	0.75	0.72	0.76	0.75	0.75	0.75
Spinel Cr/(Cr + Al)		0.49	0.51	0.41	0.52	0.52	0.47	0.50	0.52	0.49	0.50	0.49	0.50	0.44	0.45	0.45	0.45

Notes: Major elements in host rock (sample 207) were analyzed by XRF, trace elements by ICP-MS. Other elements analyzed in host rock are H_2O (5.40 wt.%), CO_2 (0.23 wt.%), Sc (46), Cr (574), Co (44), Ni (228), Cu (50), Zn (100), Ga (16), Rb (31), Nb (1.8), Mo (0.20), Sn (0.39), Cs (0.35), Pr (1.17), Tb (0.65), Ho (0.94), Tm (0.40), Lu (0.39), Hf (1.52), Ta (0.10) (all trace element concentrations in ppm). Major elements in melt inclusions and host spinel are by electron microprobe (in wt.%), trace elements by ion probe (in ppm).
na — not analyzed, bdl — concentrations below detection limit.

[a] Experiment: h — heated inclusions, u — finely re-crystallized unheated inclusions (Portnyagin et al., 2005b), u-alt — unheated altered inclusion previously described in Portnyagin et al. (2005b), strongly enriched in fluid-mobile elements (B, K, Sr, Ba, U: underlined values) compared to primary inclusions.

[b] Cr content in melt inclusion measured by ionprobe.

[c] Amount of spinel trapped during ionprobe analysis calculated as $X_{sp} = 100 \times Cr_m/Cr_{sp}$, where Cr_m is Cr content in melt inclusion measured by ionprobe, Cr_{sp} — Cr content in host spinel. All concentrations of incompatible elements measured by ionprobe were recalculated using X_{sp} and assuming negligible concentration of Cr in trapped melt.

[d] Vanadium concentrations in melt inclusions (italicized) should be considered as maximum values due to possible contamination by V-rich host spinel during analysis.

[e] Fe_2O_3 content in spinel calculated assuming ideal spinel stoichiometry.

homogenized during the heating experiments (Fig. 3B). Leaked inclusions containing a large vapor bubble and usually found in cracked grains were identified by optical investigation and excluded from further study. Quenched glasses of melt inclusions were analyzed for major elements by electron microprobe and for trace elements by ion probe.

Major elements in melt inclusions and host spinel were analyzed by Cameca SX50 microprobe at IFM-GEOMAR using at 15 kV and 10 to

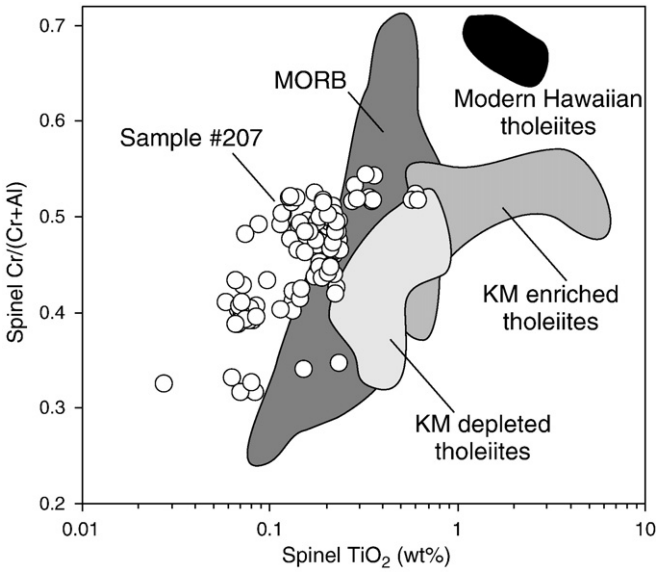

Fig. 2. Composition of chromium spinel. Spinels from Kamchatsky Mys (KM) depleted and enriched tholeiites (Portnyagin et al., 2008; Portnyagin et al., 2005b), MORB (Kamenetsky et al., 2001) and modern Hawaiian tholeiites (Sobolev and Nikogosian, 1994) are shown for comparison. Spinels from studied sample #207 extend to very low TiO_2.

30 nA for glasses and minerals, respectively. Pure oxides from Cameca and natural glasses and minerals (Jarosewich et al., 1980) were used for standardization and reference. Trace elements in melt inclusions were analyzed by Cameca ims4f ion probe at the Institute of Electronics and Informatics (Yaroslavl, Russia). Details of the analytical technique are given in Portnyagin et al. (2007) and Sobolev (1996). Glass KL-2G (Jochum et al., 2006) and NIST-610 (Rocholl et al., 1997) were used for reference during routine measurements. Accuracy and precision were estimated to be better than 10% for all elements with concentrations above 1 ppm and 10 to 30% for concentrations 0.1–1 ppm. Detection limit for most trace elements is estimated at 0.01–0.02 ppm.

Whole rock was analyzed for major, some trace elements and Sr–Nd isotopes by XRF and TIMS at IFM-GEOMAR and for trace elements by ICP-MS at the Christian-Albrecht University (Kiel, Germany). Details of the analytical techniques are given in Portnyagin et al. (2005a).

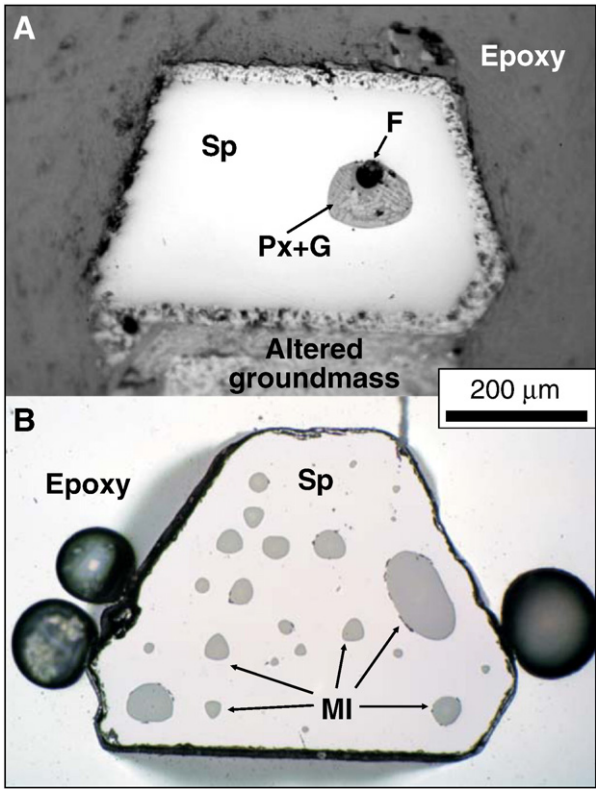

Fig. 3. Microphotographs of melt inclusions in spinel: (A) Unheated melt inclusion consisting of shrinkage fluid bubble (F) and fine aggregate of high-Ca pyroxene and glass (Px + G); (B) Melt inclusions (MI) homogenized at 1250 °C (grain #9). All inclusions in this grain have ultra-depleted compositions. Photographs were taken in polarized reflected light through an optical microscope.

4. Results

Eighty-four homogenized melt inclusions from sample #207 were analyzed for major elements by electron microprobe and 16 for trace elements by ion probe, including 5 compositions of re-crystallized inclusions previously published in Portnyagin et al. (2005b) (Table 1; Supplementary Table 1). Melt inclusions exhibit a wide range Mg# (0.52–0.71, where Mg# is molar Mg/(Mg + Fe)), which correlates only weakly with Mg# of host spinel. Significant correlations are observed between melt Mg#, inclusion size, FeO, and MgO (positive correlations) and SiO_2 and Al_2O_3 (negative correlations) (Fig.4, Supplementary Fig. 1). The most magnesian (Mg# = 0.68–0.72) and large inclusions (>40 µm in diameter) have MgO (9.0–11.3 wt.%), FeO (6.9–8.4 wt.%) and Al_2O_3 (15.0–16.8 wt.%) contents similar to primitive MORB melts (Melson et al., 1977; Langmuir et al., 1992), but generally slightly higher SiO_2 (50.3–51.8 wt.%) and CaO (13.3–14.2 wt.%) contents. Less magnesian, small, low-Fe, low-Mg and high-Al melt inclusions have drastically different major element compositions than MORB. Importantly, large variations of Mg# and major element oxides, covering the entire compositional range were found for co-genetic inclusions of different size captured in single spinel crystals, for example, for 15 inclusions of different size in grain #9 (Fig. 3B, Supplementary Fig. 2). Much of the major element variations in the melt inclusions can be explained by diffusive re-equilibration of melt inclusions with host spinel (see Section 5.1).

Concentrations of incompatible elements in melt inclusions do not correlate well with Mg#, MgO, FeO or Al_2O_3. Strong correlation exists, however, between TiO_2 (and Na_2O) in melts and TiO_2 in host spinel (Fig. 5). Concentrations of incompatible elements also exhibit a broad correlation with Mg# of host spinel (Fig.4, Supplementary Fig. 1). Inclusions in relatively low-Mg (Mg# < 0.72), high Ti (TiO_2 > 0.25 wt.%) and low-Al (Cr/(Cr + Al) = 0.51–0.53) spinels have the highest TiO_2 (0.6–1.3 wt.%), Na_2O (1.2–2.3 wt.%), K_2O (up to 0.15 wt.%) and the lowest CaO/Na_2O (6–13), which fall at the depleted end and overlap with the compositions of primitive MORB glasses (e.g., Melson et al., 1977; Langmuir et al., 1992). Inclusions in high-Mg (Mg# > 0.72) low-Ti (TiO_2 < 0.25 wt.%) and relatively Al-rich (Cr/(Cr + Al) = 0.32–0.52) spinels are highly depleted in TiO_2 (0.13–0.60 wt.%), Na_2O (0.2–1.2 wt.%), K_2O (≤0.04 wt.%) and P_2O_5 (≤0.08 wt.%). CaO/Al_2O_3 (0.82–0.92 in inclusions with Mg# > 0.68) are relatively high but comparable to primitive MORB glasses and melt inclusions in olivine from the FAMOUS/AMAR region (Melson et al., 1977; Kamenetsky, 1996; Langmuir et al., 1992; Shimizu, 1998) yet CaO/Na_2O (12–52) are considerably higher compared to MORB. Noticeably, the low-Ti melt inclusions were found in spinel phenocrysts with extremely low-Ti content not documented in mid-ocean ridge settings in the previous studies (Fig. 2, Kamenetsky et al., 2001). Sulfur concentrations are uniformly high in all inclusions (1040 ± 220 ppm, 1SD, Table 1, Supplementary Table 1) and similar to primitive MORB (Wallace and Carmichael, 1992), suggesting saturation with immiscible sulfide phase during crystallization. Chlorine content in melts is less than 100 ppm.

All inclusions analyzed for trace elements are 5 to 200 times more depleted in highly incompatible elements (e.g., La, K, Ba) and up to 3 times more depleted in moderately incompatible elements (e.g., Ti, Y)

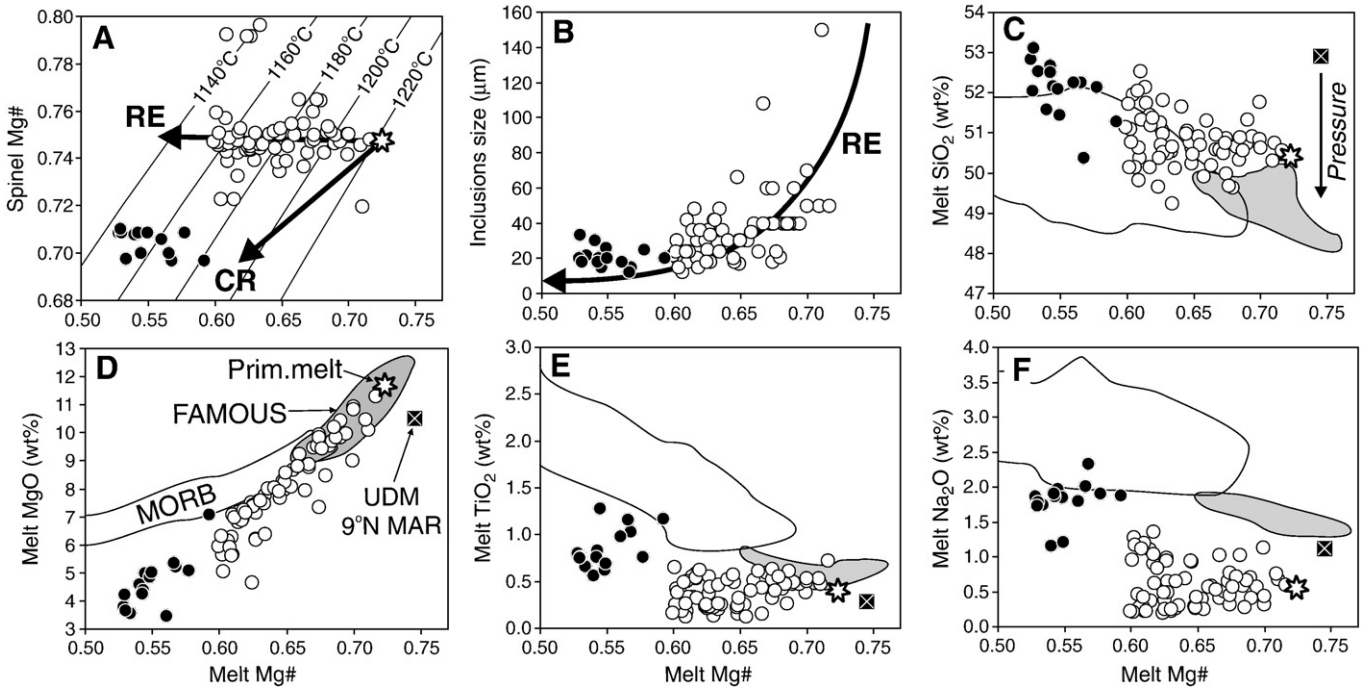

Fig. 4. Major element systematics of melt inclusions. Open circles denote composition of inclusions in the most primitive spinel crystals with Mg# > 0.6, filled circles — inclusions in spinel with Mg# < 0.6. Open star symbol shows the composition of primary melt calculated by the addition of 4% olivine to the average composition of the most high-Mg# inclusions (Mg# > 0.68) (see text for details). Compositions of MORB glasses from the East Pacific Rise (PetDB, Petrological Data Base of the Ocean Floor, http://www.petdb.org/petdbWeb/index.jsp), melt inclusions in spinel from the FAMOUS Fracture Zone (Kamenetsky, 1996) and UDM from 9°N MAR (Sobolev and Shimizu, 1993) are shown for comparison. Variations of major element compositions are ascribed to two major factors: (1) re-equilibration with host spinel which affected major spinel constituents (e.g., Mg), and (2) variations in degree of partial melting and source composition which are responsible for scatter of elements in the melts incompatible in spinel (Ti, Na) (see also Supplementary Fig. 1). In plot (A) equilibrium compositions of spinel and melt are shown, calculated using model from (Ariskin and Nikolaev, 1996) for the temperature interval 1140–1220 °C and constant $fO_2 = -9.5$, molar Si/[Si + Al] = 0.7 and $Fe^{3+}/Fe^{2+} = 0.063$ in melt. Bold arrows in (A) denote trend of re-equilibration (RE) driving melt compositions to low Mg# at decreasing temperature and constant spinel composition and expected trend of crystallization (CR) — coupled decrease of Mg# in melt and equilibrium spinel. The decrease in inclusion size with Mg# (B) is also consistent with re-equilibration. In plot (C) vertical arrow denotes decreasing Si content in mantle melts with increasing pressure of equilibrium with mantle peridotite (e.g., Langmuir et al., 1992; Kinzler and Grove, 1992).

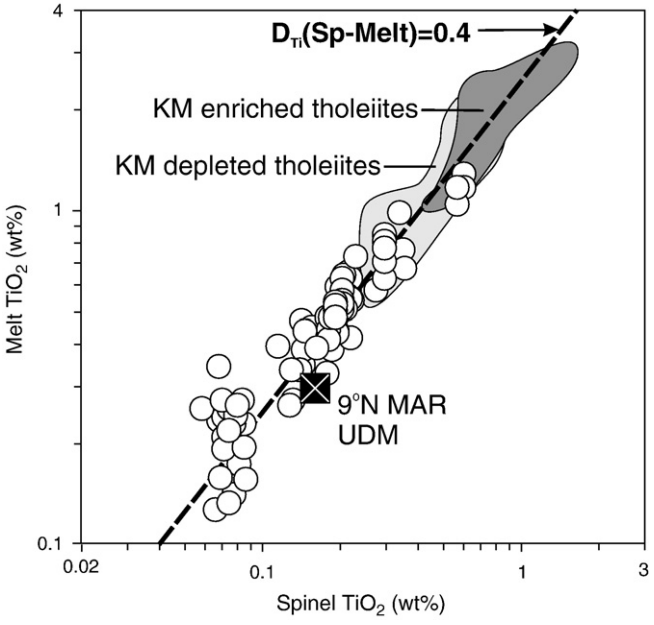

Fig. 5. Relationships between TiO_2 content in melt inclusions and host spinels. Strong linear correlation suggests equilibrium partitioning of TiO_2 between melts and host spinel and implies that extremely low-Ti compositions is a natural fact. Partition coefficient of Ti between melt and spinel estimated from this data is ~0.4. Other compositions shown are the UDM from 9°N MAR (Sobolev and Shimizu, 1993) and coexisting melts and spinels from the groups of depleted and enriched tholeiites in the Kamchatsky Mys ophiolites (Portnyagin et al., 2008; Portnyagin et al., 2005b).

compared to host rock and N-MORB (Figs. 6, 7). The most depleted inclusions have K = 1.7–8.9 ppm, Sr = 1.2–5.5 ppm, Zr = 0.9–11 ppm, La = 0.015–0.040 ppm, B = 0.011–0.024 ppm and steeply fractionated yet smooth patterns of more to less incompatible trace elements (La/Yb = 0.009–0.023, Zr/Y = 0.10–0.62, Ti/Zr = 312–1433). These compositions overlap only partially with known compositions of depleted MORB, extending to distinctly lower contents of moderately to highly incompatible elements. Less depleted inclusions have flattened REE patterns and a pronounced positive Sr anomaly (chondrite normalized $[Sr/Nd]_N = 1.2–4.1$), correlating positively with La/Sm ratio (Fig. 8).

A single ultra-depleted melt (UDM) inclusion from the Mid-Atlantic Ridge (MAR) (Sobolev and Shimizu, 1993) has been reported previously, which is similar to the most depleted melt inclusions from this study. The UDMs from the Kamchatka ophiolite, however, have higher FeO, CaO and heavy rare-earth element (HREE: Dy, Er, Yb) contents and lower Na_2O and SiO_2 (Figs. 4 and 6). All other strongly depleted melt inclusions reported previously in mid-ocean-ridge and hotspot settings (Sobolev, 1996; Sobolev et al., 2000; Shimizu, 1998; Gurenko and Chaussidon, 1995; Slater et al., 2001) have concentrations of highly incompatible elements an order of magnitude higher compared to the UDMs from the Kamchatkan ophiolites and 9°N MAR.

In order to test potential effects of secondary alteration on the composition of melt inclusions, we analyzed for major and trace elements one obviously altered inclusion containing chloritized glass (#SP8a, Table 1). This inclusion has very high concentrations of fluid-mobile elements (K, Sr, Ba, B, U) compared to primary inclusions and concentrations of fluid-immobile elements (e.g. REE, Zr, Th) well within the range of primary inclusion compositions (e.g., inclusions

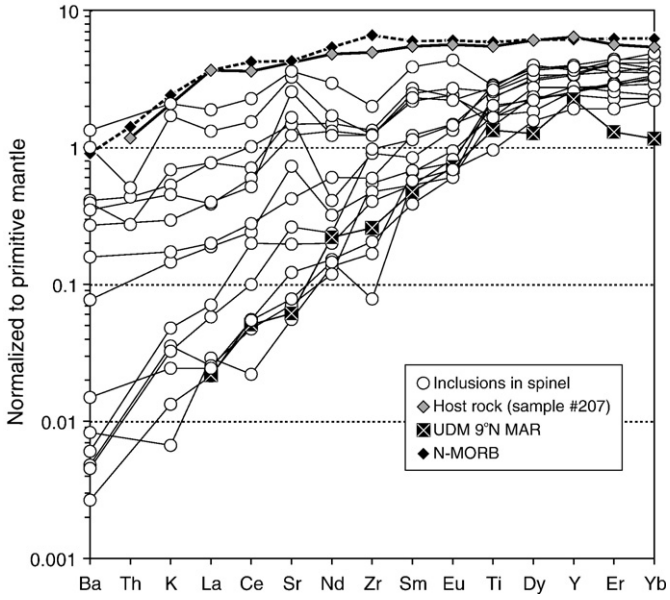

Fig. 6. Primitive-mantle-normalized concentrations of incompatible trace elements in melt inclusions range from N-MORB to ultra-depleted compositions similar (but distinct in some incompatible element contents) from ultra-depleted melt (UDM) inclusion in olivine from 9°N on the mid-Atlantic ridge (MAR) (Sobolev and Shimizu, 1993). Also shown are host rock and average N-MORB (Sun and McDonough, 1989). Normalization values are from Sun and McDonough (1989).

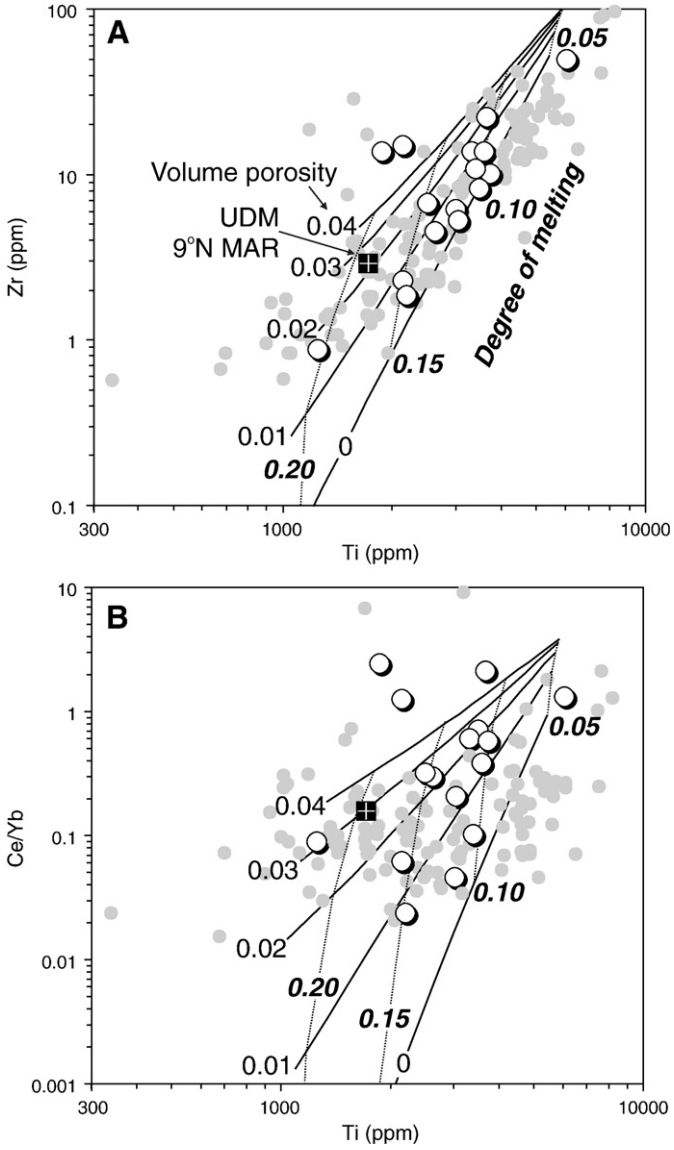

Fig. 7. Results of quantitative modeling of trace element concentrations in melt inclusions. Compositions of melt inclusions are shown by open symbols with shadow. Gray dots illustrate melt compositions in equilibrium with residual pyroxenes in abyssal mantle peridotites (Brunelli et al., 2006; Hellebrand et al., 2002; Johnson et al., 1990; Johnson and Dick, 1992) as calculated by using partition coefficients from Hart and Dunn (1993). The composition of UDM in olivine from 9°N MAR (Sobolev and Shimizu, 1993) is shown for comparison. Modeling of trace elements during mantle melting was carried out by using revised equations of dynamic melting with critical mantle porosity (Shaw, 2000). Solid lines represent melting curves at volume porosity ranging from 0 (pure fractional melting) to 0.04. Italicized bold values denote different degrees of partial melting. Dotted lines connect melt compositions produced at equal degree of partial melting (at 5% intervals) as labeled by bold italicized numbers. Model source composition is depleted MORB mantle (DMM) (Salters and Stracke, 2004). Partition coefficients for mineral phases in mantle peridotite, modal source compositions and melting reactions were used after Brunelli et al. (2006), Hellebrand et al. (2002) and references therein.

#SP8b and SP8c in the same spinel crystal, Table 1). On the basis of this observation we conclude that primary inclusions studied here were not affected by secondary alteration and can be informative about initially trapped melts.

5. Discussion

5.1. Post-entrapment modification of melt inclusions

5.1.1. Diffusive exchange with host spinel

Major elements in melt inclusions exhibit compositional trends, which are drastically different from cotectic MORB compositions (Fig. 4, Supplementary Fig. 1). Apparently, crystallization of olivine + spinel (± plagioclase ± pyroxene) assemblage from parental MORB-like melts cannot explain coupled increase Al, Ca, Si and decrease Mg and Fe in these melt inclusions. These trends also cannot be generated by melting of host spinel during experimental reheating.

Alternatively, we propose that the large compositional range of melt inclusions can be in part explained by diffusive re-equilibration of melt inclusions with host spinel. This process has been proposed in several previous works to affect significantly the composition of spinel-hosted inclusions (Kamenetsky et al., 2002; Shimizu et al., 2001; Spandler et al., 2000; Zlobin et al., 1990). There are three major lines of evidence for post-entrapment re-equilibration of melt inclusions with host spinel: (1) correlation of melt composition with inclusion size, (2) constant amount of spinel constituent components in melts, and (3) diffusive zoning around melt inclusions.

The inclusions exhibit clear size-dependent compositional variations (Fig. 4B, Supplementary Figs. 1 and 2). Small inclusions are noticeably depleted in Fe and Mg, enriched in Al and Cr and have low Mg# compared to larger inclusions. Importantly, large inclusions have compositions closer to equilibrium with host spinel than small inclusions. We interpret this correlation as evidence for more extensive re-equilibration of inclusions of smaller size, because these inclusions are expected to re-equilibrate faster than large inclusions (Danyushevsky et al., 2000; Qin et al., 1992).

Inclusions affected by entrapment of the boundary layer melt around the growing crystal (Roedder, 1984) also can exhibit size-dependent compositional variations. This, however, cannot explain the data in Fig. 4. Because host spinels have higher Al_2O_3 content than melt inclusions, the boundary layer melt and small inclusions should be depleted in Al, not enriched, as we observe for the studied inclusions.

When co-genetic inclusions in single spinel crystals are examined, the total amount of the major spinel constituent components (Mg, Fe, Al and Cr) in the inclusions remains constant within only 2–3 atomic (at.) %. This observation implies that enrichment in Al and Cr and depletion in Mg and Fe almost balance each other. The balance is a

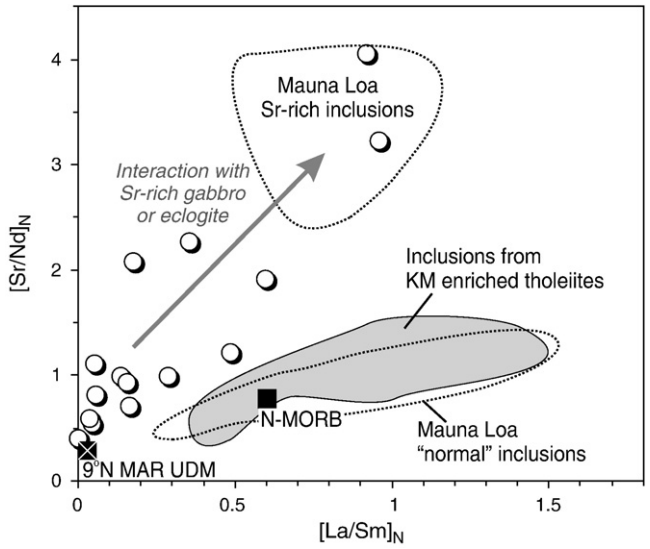

Fig. 8. Correlation between mantle-normalized (after Sun and McDonough (1989)) Sr/Nd and La/Sm ratios in melt inclusions. The UDM inclusions from sample #207 exhibit a positive correlation toward compositions of Sr-rich melts from Mauna Loa volcano (Sobolev et al., 2000). This trend can be explained either by assimilation of crustal gabbro (Danyushevsky et al., 2003; Gurenko and Sobolev, 2006) or by mixing of UDMs (low Sr/Nd) and high-Sr LREE-rich melts from recycled eclogitized gabbro within the plume (Sobolev et al., 2000).

characteristic feature of the iso-cation exchange between melt and spinel in a closed system. Weak decrease of the total amount of spinel components and increase of SiO_2 content in highly re-equilibrated low-Mg inclusions suggests that the re-equilibration process could concur with crystallization of a small amount of spinel on inclusion walls, which could lead to Si enrichment.

Additional argument for the partial re-equilibration is specific diffusive zoning of host spinel around melt inclusions, which we found to be as wide as ~10 μm for 80 μm-large inclusions (Supplementary Fig. 3). Toward melt inclusion interface, MgO, Fe_2O_3, Mg# in host spinel increase and FeO, Al_2O_3, Cr_2O_3 and Fe^{2+}/Fe^{3+} decrease. These compositional gradients suggest that Al, Cr and Fe^{2+} migrated from spinel into melt, and Mg and Fe^{3+} migrated from melt into spinel after isolation of melt inclusion from matrix melt.

Summarizing the chemical data, re-equilibration of the melt inclusions with host spinel should have involved the following reactions:

$$MgO_{melt} + FeO_{sp} = MgO_{sp} + FeO_{melt} \quad (1)$$

$$Fe_2O_{3\,melt} + Al_2O_{3\,sp} = Fe_2O_{3\,sp} + Al_2O_{3\,melt} \quad (2)$$

$$Fe_2O_{3\,melt} + Cr_2O_{3\,sp} = Fe_2O_{3\,sp} + Cr_2O_{3\,melt} \quad (3)$$

$$2FeO_{melt} + 3O_{2\,melt} = 2Fe_2O_{3\,melt} \quad (4)$$

Some of the reactions have been proposed to explain compositional peculiarities of melt inclusions in spinel (e.g., Kamenetsky et al., 2002; Shimizu, 1998; Zlobin et al., 1990). Here we show that the process is more complex and involves virtually all major spinel constituent components.

Equilibrium constant for the reaction (1) is temperature dependent so that melt in equilibrium with spinel of constant composition should be less magnesian at lower temperature (Fig. 4; Ariskin and Nikolaev, 1996). Therefore, re-equilibration in respect to Mg and Fe is likely to have occurred with decreasing temperature in the magma chamber prior to eruption. Reactions (2) and (3) involve Fe^{3+} in melt exchanging with Al and Cr in spinel. Excess amount of Al and Cr in substantially re-equilibrated inclusions is about 1.5 at.%, which implies that inclusions lost equal molar amount of Fe^{3+}. This amount of Fe^{3+} exceeds significantly the available amount of Fe^{3+} in melt (~0.25 at.%) at reduced conditions of crystallization (mean Fe^{2+}/Fe^{3+}~13 in melts as calculated from composition of spinels following the method in Maurel and Maurel (1982)). Therefore, reaction of iron oxidation in melt (4) also should accompany the cation exchange between spinel and melt, probably, reflecting evolution of melt in equilibrium with spinel of constant composition at decreasing temperature and constant oxygen fugacity.

The complexity of the exchange reactions between melt and spinel makes it difficult to model the process quantitatively. A key observation from our results, however, is that melt Mg# decreases substantially during re-equilibration. Therefore, the melts with the highest Mg# should have been the least affected by the re-equilibration. Some inclusions from this study have Mg# as high as 0.68–0.73, approaching compositions of parental mantle-derived magmas. These inclusions are believed to preserve nearly unchanged initial melt compositions and can be used to estimate conditions of equilibria with mantle residue. Concentrations of elements incompatible to spinel (e.g., Ca, Na, Ti, REE etc.) do not correlate with melt Mg# (Fig. 4, Supplementary Fig. 1) and, therefore, have been likely not affected by the re-equilibration with host spinel.

5.1.2. Diffusive exchange with matrix melt

Diffusive exchange between melt inclusions and surrounding melt through host mineral has been proposed to modify concentrations of incompatible elements in melt inclusions hosted by olivine and spinel on time scale of tens to hundreds years (Spandler et al., 2007). Expected effect of this process is two-fold: (1) composition of inclusions approaches matrix melt as re-equilibration proceeds, and (2) concentrations of elements with similar diffusivity but with different partition coefficients between host mineral and melt should fractionate during partial re-equilibration (Qin et al., 1992).

The range of UDM inclusions is particularly large (Fig. 6) and might be thought to reflect variable re-equilibration with matrix melt. It is however noticeable that trace elements with contrasting partition coefficients with respect to spinel (for example, Dy and Ti) strongly correlate in the UDM inclusions. If the re-equilibration would have affected the trace element composition of these inclusions, this should result in disturbed correlation between REE and Ti. Titanium is much more compatible in spinel than Dy (D_{Ti}~0.4, this study, Fig. 5; D_{Dy}~D_{Tb} = 0.0009, (Spandler et al., 2007)) and should achieve re-equilibration ~2 orders of magnitude faster compared to REE, even if the diffusivity of Dy and Ti is similar in spinel (Qin et al., 1992). Melt inclusions studied here including UDMs do not exhibit anomalously high Ti/HREE ratios, expected from partial re-equilibration with matrix melt (Fig. 6). Therefore, we conclude that the processes of diffusive re-equilibration with matrix melt did not significantly affect compositions of studied inclusions. This implies a very short residence time (not more than a few months) of the spinel phenocrysts with UDM inclusions in MORB-like matrix melt prior to eruption.

5.2. Hypotheses of the UDM origin

The ultra-depleted composition of melt inclusions implies specific conditions of magma generation. Possible explanations include: (1) re-melting of depleted mantle residues in a subduction-related environment (Duncan and Green, 1980; Crawford et al., 1989) or at a ridge axis (Benoit et al., 1999), (2) melting of trace element poor crustal material (Danyushevsky et al., 2003), and (3) near-fractional mantle melting and limited magma mixing during transport to the crust (Sobolev and Shimizu, 1993; Spiegelman and Kelemen, 2003).

The UDM inclusions from the Kamchatka ophiolite are depleted in Ti, Zr, Na and middle-REE (Nd, Sm, Eu) similar to boninitic melt inclusions and glasses presumably originating from a second-stage melting of MORB or ocean–island–basalt (OIB) mantle residues in subduction-related environments (Crawford et al., 1989; Portnyagin et al., 1996). Boninites are characterized by high SiO_2 and a strong enrichment in refractory (e.g., spinel Cr# = 0.7–0.9) and fluid-mobile elements and volatiles (e.g. H_2O, Cl, K, Ba, U, and Sr). Similar geochemical features also are expected for magmas originating by re-melting of serpentinized mantle peridotites at ridge axes (Benoit et al., 1999). In contrast to boninites, moderately low Cr# of host spinels (Fig. 2) and moderately low SiO_2 but high CaO and Al_2O_3 in Kamchatka melt inclusions (Fig. 4, Supplementary Fig. 1) suggest a fertile lherzolitic source (e.g., Falloon and Danyushevsky, 2000). Furthermore, these melts have very low primary contents of fluid-mobile elements (e.g., K, B, Cl and Ba; Table 1) and do not exhibit subduction-related trace element signatures, e.g. enrichment in large ion lithophile elements (LILE) relative to high field strength elements (HFSE) (Fig. 6). These features are inconsistent with an origin by re-melting of MORB residues under hydrous conditions in subduction-related settings or at a ridge axis.

Some exotic UDM inclusions in MORB were explained by melting of trace element poor minerals (e.g., plagioclase) (Danyushevsky et al., 2003). Such inclusions have high Al_2O_3, very low S and TiO_2 contents and exhibit a strong strontium-enrichment relative to other incompatible elements. These exotic melts are geochemically quite different from the melt inclusions studied here with smooth primitive-mantle-normalized trace element spectra, high S content (1040 ± 220 ppm, 1SD) and major element composition broadly similar to primitive MORB. It is also noticeable that UDM in the studied sample are very abundant (71 of 84 inclusions analyzed have $Na_2O < 1.5$ wt.%), while previously described exotic melts are usually sole inclusions associated with inclusions of typical MORB composition (Danyushevsky et al., 2003).

Since second-stage melting of hydrated residual mantle or cryptic crustal assimilation cannot easily explain the geochemical features of the inclusions, they are likely to have formed by mantle melting at very low mantle porosity (1–2% by volume) and limited mixing of variably depleted melts during their transport to the crust, as proposed previously to explain the occurrence of ultra-depleted melt inclusions in MORB phenocrysts (e.g., Sobolev and Shimizu, 1993; Gurenko and Chaussidon, 1995; Sobolev, 1996; Slater et al., 2001). This conclusion is supported by the close compositional similarity of the UDMs from Kamchatkan ophiolites and melts in equilibrium with the most depleted abyssal mantle peridotites (Fig. 7) and by the results of our quantitative modeling explained in the following chapter. This modeling emphasizes also some important compositional features distinguishing the Kamchatka UDMs from the previously published UDM from MORB and suggesting a more complex scenario of mantle melting.

5.3. Quantitative constraints on mantle melting

In order to estimate possible pressure and temperature of UDMs in equilibrium with residual mantle peridotite, we calculated the average composition of the most Mg#-rich melt inclusions (Table 2). This composition has ~10.2 wt.% MgO and can be in equilibrium with olivine having Fo88.3, marginally too low Fo for high-degree partial melt from mantle peridotite (Fo 90.5–91.5, e.g., (Herzberg et al., 2007)). This composition also is characterized by a poor agreement between pressure estimates made from different projections (olivine, plagioclase, quartz, and pyroxene) of the basaltic tetrahedron (standard deviation for four estimates is 0.67 GPa from the mean value of 0.72 GPa) (Kinzler and Grove, 1992). More consistent pressure estimates were obtained after incremental addition of ~5 wt.% olivine to the average composition of primitive melt inclusions, increasing MgO to 11.7 wt.%. This melt is in equilibrium with olivine having Fo89.7, has a liquidus olivine temperature of 1260 °C at 1 atm and could be in equilibrium with mantle lherzolite at 0.75 ± 0.25 GPa (Kinzler and Grove, 1992) and temperature of ~1300 °C (assuming the slope of olivine liquidus to be 5 °C/kbar (Ford et al., 1983)). We assume these conditions to be informative about the last equilibria of the UDMs with mantle peridotite before melt segregation and transport to the surface.

Table 2
Average composition of parental melts and mantle melting conditions.

	1	2	3
	Avg KM UDM	KM UDM PM	9°N MAR UDM
SiO_2, wt.%	50.8	50.4	52.9
TiO_2	0.49	0.47	0.29
Al_2O_3	16.0	15.3	15.5
FeO	7.93	8.04	7.03
MnO	0.10	0.10	0.08
MgO	10.2	11.7	10.5
CaO	13.8	13.3	12.5
Na_2O	0.63	0.61	1.12
K_2O	0.02	0.02	0
Fo (mol %)[a]	88.4	89.7	89.9
T (°C)[b]	1221	1260	1235
P_m (GPa)[c]		0.75 ± 0.25	0.46 ± 0.16
T_m (°C)[d]		1300 ± 13	1255 ± 8
F[e]		~20	~17
T_p (°C)[f]		~1400	~1350

Notes: 1 (Avg KM UDM) — average composition of 13 melt inclusions with Mg# > 0.68; 2 (KM UDM PM) — average primary UDM calculated by addition of 5% olivine to the composition #1; 3 (9°N MAR UDM) — composition of UDM from 9°N MAR (Sobolev and Shimizu, 1993).

[a] Liquidus olivine composition calculated by model from Ford et al. (1983).

[b] Olivine liquidus temperature at 1 atm pressure calculated by model from Ford et al. (1983).

[c] Pressure of equilibrium with lherzolite residue calculated after Kinzler and Grove (1992).

[d] Temperature of equilibrium with mantle residue calculated assuming slope of olivine liquidus 5 °C/0.1 GPa (Ford et al., 1983).

[e] Degree of depleted mantle melting estimated from trace element modeling.

[f] Potential mantle temperature estimated from T_m, P_m and F following model of perfect fractional melting of adiabatically upwelling mantle after Iwamori et al. (1995).

The estimated temperature, however, is a very minimum temperature, because FeO in the primitive melt inclusions could have been lowered relative to initial values by re-equilibration with the host spinel (chapter 5.1). Higher FeO content in primitive melt inclusions will result in higher MgO in equilibrium with olivine of equal Fo, yielding higher liquidus and mantle temperature estimates (Ford et al., 1983; Herzberg et al., 2007). Somewhat more forsteritic liquidus olivine (up to Fo91–92; Portnyagin et al. (2005b)) and consequently up to ~80 °C higher temperature for the UDMs is also predicted by semi-quantitative method proposed by Kamenetsky et al. (2001) using co-variation of Mg# and Cr# in spinel hosting melt inclusions.

The estimated pressure of UDM equilibria with mantle peridotite (~0.75 GPa) is lower than usually discussed for MORB generation (1–2 GPa, (Kinzler and Grove, 1992; Langmuir et al., 1992), but comparable to that estimated for UDM from 9°N MAR (~0.5 GPa, Table 2 (Sobolev and Shimizu, 1993)). Therefore the UDM could be the last fraction of melt produced in an upwelling mantle column, representing the highest degrees of mantle melting at shallowest sub-lithospheric depth. An important new result from our study is that UDM inclusions in early crystallizing minerals can be very abundant, which we interpret as evidence for the transport of significant amounts of nearly instantaneous mantle melts to shallow crustal depths. The abundance of UDM melt inclusions in the studied sample strongly supports magma transport in the Earth's mantle in channelized systems (Kelemen et al., 1995; Slater et al., 2001). These systems are likely to consist of interconnected networks of high-porosity dunite channels in low-porosity upwelling mantle (Kelemen et al., 1995), which also provides a mechanism for preservation of much of the chemical variability produced during

melting (Spiegelman and Kelemen, 2003). The studied inclusions could thus represent shallow mantle melts transported at the edge of a deeply nucleated channel. Alternatively, the highly depleted melts could be delivered to the crust within a separate channel(s), not connected to the main network at shallow depth (Spiegelman and Kelemen, 2003).

Quantitative modeling of trace element abundances (Fig. 7) reveals important details of the melting scenario for the origin of UDMs. This modeling illustrates that the UDMs can be only generated at very low residual mantle porosity of about 1–2%. In this respect, our results concur with the conclusions of previous workers about the very high permeability of the Earth's mantle, inferred from studies of U-series isotopes (McKenzie, 1985), experimental data (Riley and Kolhstedt, 1991), compositions of residual pyroxene in mantle peridotites (Brunelli et al., 2006; Hellebrand et al., 2002; Johnson et al., 1990; Johnson and Dick, 1992) and studies of melt inclusions in early crystallizing minerals (e.g., Gurenko and Chaussidon, 1995; Slater et al., 2001; Sobolev and Shimizu, 1993; Sobolev, 1996). On the other hand, the high degrees of melting inferred for the UDMs from a Kamchatkan ophiolite (up to ~20%) appear to be too high compared to the typical degrees of melting beneath the mid-oceanic ridges (6–15%, (Salters and Stracke, 2004; Workman and Hart, 2005)). These results are also in agreement with a relatively high temperature (≥1300 °C) of UDM equilibria with mantle residue, which is ≥45 °C higher than estimated for the UDM from 9°N MAR (1255 °C, Table 2) assuming melting of a common MORB mantle (Sobolev and Shimizu, 1993). Both high degrees of melting and high temperature of equilibrium with mantle at shallow pressure imply a high potential temperature (T_p) of the UDM mantle source with $T_p \geq 1400$ °C (Iwamori et al., 1995), at the upper limit or higher than expected for the ambient upper mantle ($T_p = 1280–1400$ °C, (Herzberg et al., 2007)). Therefore the onset of melting of hotter mantle must have occurred at greater depths and resulted at greater extent of melting than for the generation of common MORB.

5.4. A possible link to the Hawaiian hotspot

Several previous workers have proposed that the Kamchatsky Mys ophiolites represent fragments of oceanic lithosphere formed through interaction of a plume with the former Kula-Pacific spreading center in the Cretaceous (Khotin and Shapiro, 2006; Portnyagin et al., 2005b; Saveliev, 2003). This conclusion was based on the recognition of a peculiar assemblage of rock types preserved in the ophiolites, including depleted to enriched tholeiites and alkali basalts, and the belief that a seamount or thickened oceanic crust formed by plume–ridge interaction would be easier to accrete than normal oceanic crust. Possible preservation of accreted Hawaiian seamounts in eastern Kamchatka was firstly suggested in Avdeiko (1980). Based on the Cretaceous age of the ophiolites and available paleotectonic reconstructions, a genetic link between the Kamchatsky Mys ophiolites and the Hawaiian hotspot was postulated (Saveliev, 2003). A recent study of the group of enriched tholeiites from the ophiolites (Portnyagin et al., 2008) provided strong arguments supporting this idea and demonstrated that some ophiolite rocks are very similar geochemically to those recovered from the Cretaceous Emperor Seamounts, Detroit and Meiji, and the Hawaiian Islands, Mauna Kea and Mauna Loa. It was concluded that the ophiolitic basalts represent Early to middle Cretaceous products of the Hawaiian hotspot (Portnyagin et al., 2008), which was located near an oceanic spreading center at that time (Keller et al., 2000; Regelous et al., 2003).

The compositions of host rock and UDM inclusions studied here are very different from the enriched tholeiites described in Portnyagin et al. (2008) and cannot originate from the same mantle source. There are, however, several lines of evidence that the hot Hawaiian mantle plume could strongly influence and possibly promote extensive mantle melting required to generate the UDMs reported here.

The potential mantle temperature of the UDM source (≥1400 °C), which is required to explain the high liquidus temperature of UDMs at shallow depths (≥1260 °C) and high degrees of melting (up to 20% at 20 km depth) of the mantle source, is at the upper limit of the ambient upper mantle with $T_p = 1280–1400$ °C (Herzberg et al., 2007). In this respect, the origin of UDMs from Kamchatka might be similar to the origin of depleted MORBs in anomalous segments of mid-ocean ridges affected by hotspots, for example, Reikjanes Ridge and FAMOUS/AMAR region of the Mid-Atlantic Ridge (Dosso et al., 1999; Herzberg et al., 2007; Slater et al., 2001).

Two explanations for the high temperature of the UDM mantle source are that the source mantle represents an ambient mantle entrained and heated by a hot plume or a depleted part of a hot upwelling mantle plume. These hypotheses are difficult to reconcile with the presently available data. On the one hand, the Hawaiian plume was shown to have very high T_p ~1550 °C (Herzberg et al., 2007; Sobolev and Nikogosian, 1994; Sobolev et al., 2005). Therefore significant heating of ambient or entrained mantle can be a plausible consequence of interaction of the Hawaiian plume with upper oceanic mantle, as has been proposed to explain the presence of a depleted component in the Cretaceous Hawaiian plume (Keller et al., 2000) and the Icelandic plume (Kempton et al., 2000).

Alternatively, the UDM source can represent a depleted part of mantle plume (Huang et al., 2005; Regelous et al., 2003). Although the estimated T_p of the UDM source appears to be too low for the Hawaiian plume, supporting evidence for the possible origin of the UDMs by melting of the Hawaiian plume is the occurrence of Ba- and Sr-rich inclusions, which may reflect characteristics of their mantle source ((Portnyagin et al., 2005b), Figs. 6 and 8). The flattened trace element patterns and positive Sr-anomalies in the least depleted melt inclusions from Kamchatka can be explained by mixing of the UDM and LREE- and Sr-rich melts found as inclusions in Mauna Loa olivines (Fig. 8), interpreted to be melts from recycled lower gabbroic oceanic crust in the Hawaiian plume (Sobolev et al., 2000). Such melts could be generated within the same mantle column and mix with depleted melts from mantle peridotite as could be expected from extensive mantle plume melting beneath thin lithosphere (Huang et al., 2005; Regelous et al., 2003).

In conclusion, we propose that an unusual suite of melt inclusions including UDM in spinel from basalt from the Kamchatka Cape ophiolite originates through extensive melting of depleted mantle, which could be intrinsic to the Hawaiian plume ("depleted plume component") or entrained (e.g., at 670 km discontinuity (Kempton et al., 2000)) depleted upper mantle heated by the plume. Judging from results of Portnyagin et al. (2008) and this study, the period of interaction of the Hawaiian plume with an ocean ridge and generation of depleted magmas was likely relatively long, from at least ~100 Ma (Kamchatka Cape ophiolite) to 76–81 Ma (Detroit seamount (Duncan and Keller, 2004)). Whereas modern Hawaiian magmas originate through relatively small degrees of melting, limited by thick lithosphere, and are fed largely from more-easily melted pyroxenitic sources (Herzberg, 2006; Sobolev et al., 2005), the UDM studied here require a large contribution from more refractory peridotitic, possibly plume source material, and thus can be informative of the depleted end-member within the Hawaiian plume, proposed in a number of previous studies (Huang et al., 2005; Regelous et al., 2003) but not sampled directly.

6. Conclusions

We have carried a detailed study of major and trace element composition of spinel-hosted melt inclusions from Cretaceous MORB-like olivine–plagioclase phyric basalt in the Kamchatsky Mys ophiolites (Eastern Kamchatka). These ophiolites represent fragments of oceanic lithosphere, shown previously to originate through interaction of the Hawaiian plume and a spreading ridge and to host

rocks akin to the Cretaceous Hawaiian tholeiites from the Meiji and Detroit Seamounts. Our results are summarized as follows:

1) Melt inclusions in spinel span a wide compositional range, originating from the initial diversity of captured melts and subsequent partial re-equilibration of inclusions with the host spinel. The re-equilibration occurred through iso-cation exchange with the host spinel and affected major elements in melt inclusions, particularly major constituents of spinel (Mg, Fe, Al, and Cr). Major and trace elements in inclusions that are incompatible in spinel were not obviously affected by the re-equilibration process and are informative about conditions of magma generation.
2) Melt inclusion compositions range from those that are similar to the most depleted MORB glasses to those that are ultra-depleted in incompatible elements, only comparable to a single melt inclusion in olivine from 9°N MAR (Sobolev and Shimizu, 1993). The UDM melts formed at shallow mantle depth (~20 km) as a result of polybaric, near-fractional melting of depleted mantle with $T_p \geq 1400$ °C and thus represent the last melt fractions generated in an upwelling column of mantle, which began melting at ≥75 km depth.
3) The abundance of UDM inclusions in the studied sample strongly supports magma transport in the Earth's mantle in channelized systems, allowing preservation of large chemical heterogeneity of mantle melts during their transport to the crust. The studied inclusions can represent shallow mantle melts transported at the edge of a deeply nucleated dunite channel or within a separate channel(s) disconnected from the main network at shallow depth.
4) The presence of melts ranging in composition from ultra-depleted to Mauna Loa-like, high-T mantle source and association with rocks sharing peculiar geochemical features with the Cretaceous Hawaiian tholeiites (from Meiji and Detroit Seamounts) suggest that the suite of highly depleted melts from the Kamchatkan ophiolites originated through extensive melting of a heterogeneous mantle source, which could be intrinsic to the Hawaiian plume ("depleted plume component") or upper mantle entrained and heated at the plume margins.

Finally, we emphasize the great potential of using melt inclusions in spinel, a common accessory mineral in primitive basalts, to decipher the composition of parental magmas of old and highly altered volcanic rocks preserved in ophiolites, providing unique information about the origin and history of oceanic magmatism on Earth.

Acknowledgement

We thank M. Thöner and S. Simakin for their generous help with the electron microprobe and ionprobe analyses. This work benefited from critical comments from T. Kokfelt, C. Herzberg, A. Sobolev and V. Kamenetsky. We gratefully thank the Deutsche Forschungsgemeinschaft (DFG, Ho1833/14-1) and Bundes Ministerium für Bildung und Forschung (KALMAR project) for providing funding to M.P. and K. H. and the Russian Foundation for Basic Research (RFBR, 07-05-00080) for funding to D.S.

Appendix A. Supplementary data

Supplementary data associated with this article can be found, in the online version, at doi: 10.1016/j.epsl.2009.07.042.

References

Ariskin, A.A., Nikolaev, G.S., 1996. An empirical model for the calculation of spinel–melt equilibria in mafic igneous systems at atmospheric pressure: 1. Chromian spinels. Contrib. Mineral. Petrol. 123, 282–292.
Avdeiko, G.P., 1980. On possible continuation of the Hawaiian-Emperor chain in Kamchatka, DSDP Leg 55, Initial Reports of the Deep Sea Drilling Project. Government Printing Office, Washington, U.S, pp. 851–854.
Benoit, M., Ceuleneer, G., Polve, M., 1999. The remelting of hydrothermally altered peridotite at mid-ocean ridges by intruding mantle diapirs. Nature 402, 514–518.
Brunelli, D., Seyer, M., Ciprani, A., Ottolini, L., Bonatti, E., 2006. Discontinuous melt extraction and weak refertilization of mantle peridotites at the Vema lithospheric section (Mid-Atlantic Ridge). J. Petrol. 47, 745–771.
Crawford, A.J., Falloon, T.J., Green, D.H., 1989. Classification, petrogenesis and tectonic setting of boninites. In: Crawford, A.J. (Ed.), Boninites. Unwin Hyman, London, pp. 1–49.
Danyushevsky, L.V., Della-Pasqua, F.N., Sokolov, S., 2000. Re-equilibration of melt inclusions trapped by magnesian olivine phenocrysts from subduction-related magmas: petrological implications. Contrib. Mineral. Petrol. 138, 68–83.
Danyushevsky, L.V., Perfi, M.R., Eggins, S.M., Falloon, T.J., 2003. Crustal origin for coupled 'ultra-depleted' and 'plagioclase' signatures in MORB olivine-hosted melt inclusions: evidence from the Siqueiros Transform Fault, East Pacific Rise. Contrib. Mineral. Petrol. 144, 619–637.
Dick, H.B.J., Bullen, T., 1984. Chromian spinel as a petrogenetic indicator in abyssal and alpine-type peridotites and spatially associated lavas. Contrib. Mineral. Petrol. 86, 54–76.
Dosso, L., Bougault, H., Langmuir, C., Bollinger, C., Bonnier, O., Etoubleau, J., 1999. The age and distribution of mantle heterogeneity along the Mid-Atlantic Ridge (31–41°N). Earth Planet. Sci. Lett. 170, 269–286.
Duncan, R.A., Green, D.H., 1980. Role of multi-stage melting in the formation of oceanic crust. Geology 8, 22–26.
Duncan, R.A., Keller, R.A., 2004. Radiometric ages for basement rocks from the Emperor Seamounts, ODP Leg 197. Geochem. Geophys. Geosyst. 5, Q08L03. doi:10.1029/2004GC000704.
Falloon, T.J., Danyushevsky, L.V., 2000. Melting of refractory mantle at 1.5, 2 and 2.5 GPa under anhydrous and H_2O-undersaturated conditions: implications for the petrogenesis of high-Ca boninites and the influence of subduction components on mantle melting. J. Petrol. 412, 257–283.
Fedorchuk, A.V., 1992. Oceanic and back-arc basin remnants within accretionary complexes: geological and geochemical evidence from Eastern Kamchatka. Ofioliti 17, 219–242.
Ford, C.E., Russel, D.G., Graven, J.A., Fisk, M.R., 1983. Olivine-liquid equilibria: temperature, pressure and composition dependence of the crystal/liquid cation partition coefficients for Mg, Fe^{2+}, Ca and Mn. J. Petrol. 24, 256–265.
Gurenko, A., Sobolev, A., 2006. Crust–primitive magma interaction beneath neovolcanic rift zone of Iceland recorded in gabbro xenoliths from Midfell, SW Iceland. Contrib. Mineral. Petrol. 151, 495–520.
Gurenko, A.A., Chaussidon, M., 1995. Enriched and depleted primitive melts included in olivine from Icelandic tholeiites: origin by continuous melting of single mantle column. Geochim. Cosmochim. Acta 59, 2905–2917.
Hart, S.R., Dunn, T., 1993. Experimental cpx/melt partitioning of 24 trace elements. Contrib. Mineral. Petrol. 113, 1–8.
Hauff, F., Hoernle, K., van den Bogaard, P., Alvarado, G., Garbe-Schönberg, D., 2000. Age and geochemistry of basaltic complexes in western Costa Rica: contributions to the geotectonic evolution of Central America. Geochem. Geophys. Geosyst. 1 (5). doi:10.1029/1999GC000020.
Hellebrand, E., Snow, J.E., Hoppe, P., Hofmann, A.W., 2002. Garnet-field melting and late-stage refertilisation in 'residual' abyssal peridotites fromthe Central Indian Ridge. J. Petrol. 43, 2305–2338.
Herzberg, C., 2006. Petrology and thermal structure of the Hawaiian plume from Mauna Kea volcano. Nature 444, 605–609.
Herzberg, C., Asimow, P.D., Arndt, N., Niu, Y., Lesher, C.M., Fitton, J.G., Cheadle, M.J., Saunders, A.D., 2007. Temperatures in ambient mantle and plumes: constraints from basalts, picrites, and komatiites. Geochem. Geophys. Geosyst. 8, Q02006. doi:10.1029/2006GC001390.
Hofmann, A.W., Jochum, K.P., 1996. Source characteristics derived from very incompatible trace elements in Mauna Loa and Mauna Kea basalts, Hawaii Scientific Drilling Project. J. Geophys. Res. 101, 11831–11839.
Huang, S., Frey, F.A., 2003. Trace element abundances of Mauna Kea basalt from phase 2 of the Hawaii Scientific Drilling Project: petrogenetic implications of correlations with major element content and isotopic ratios. Geochem. Geophys. Geosyst. 4 (6).
Huang, S., Regelous, M., Thordarson, T., Frey, F.A., 2005. Petrogenesis of lavas from Detroit Seamount: geochemical differences between Emperor Chain and Hawaiian volcanoes. Geochem. Geophys. Geosyst. 6, Q01L06. doi:10.1029/2004GC000756.
Iwamori, H., McKenzie, D., Takahashi, E., 1995. Melt generation by isentropic mantle upwelling. Earth Planet. Sci. Lett. 134, 253–266.
Jarosewich, E.J., Nelen, J.A., Norberg, J.A., 1980. Reference samples for electron microprobe analysis. Geostand. Newsl. 4, 43–47.
Jochum, K.P., et al., 2006. MPI-DING reference glasses for in situ microanalysis: new reference values for element concentrations and isotope ratios. Geochem. Geophys. Geosyst. 7. doi:10.1029/2005GC001060.
Johnson, K.T.M., Dick, H.J.B., 1992. Open system melting and temporal and spatial variation of peridotite and basalts at the Atlantis II Fracture Zone. J. Geophys. Res. 97, 9219–9241.
Johnson, K.T.M., Dick, H.J.B., Shimizu, N., 1990. Melting in the oceanic upper mantle: an ion microprobe study of diopsides in abyssal peridotites. J. Geophys. Res. 95, 2661–2678.
Kamenetsky, V.S., 1996. Methodology for the study of melt inclusions in Cr-spinel, and implications for parental melts of MORB from FAMOUS area. Earth Planet. Sci. Lett. 142, 479–486.
Kamenetsky, V.S., Crawford, A.J., Meffre, S., 2001. Factors controlling chemistry of magmatic spinel: an empirical study of associated olivine, Cr-spinel and melt inclusions from primitive rocks. J. Petrol. 42, 655–671.

Kamenetsky, V.S., Sobolev, A.V., Eggins, S.M., Crawford, A.J., Arculus, R.J., 2002. Olivine-enriched melt inclusions in chromites from low-Ca boninites, Cape Vogel, Papua New Guinea: evidence for ultramafic primary magma, refractory mantle source and enriched components. Chem. Geol. 183, 287–303.

Kelemen, P.B., Shimizu, N., Salters, V.J.M., 1995. Extraction of mid-ocean-ridge basalt from the upwelling mantle by focused flow of melt in dunite channels. Nature 375, 747–753.

Keller, R.A., Fisk, M.R., White, W.M., 2000. Isotopic evidence for Late Cretaceous plume–ridge interaction at the Hawaiian hotspot. Nature 405, 673–676.

Kempton, P.D., Fitton, J.G., Saunders, A.D., Nowell, G.M., Taylor, R.N., Hardarson, B.S., Pearson, G., 2000. The Iceland plume in space and time: a Sr–Nd–Pb–Hf study of the North Atlantic rifted margin. Earth Planet. Sci. Lett. 177, 255–271.

Khotin, M.Y., Shapiro, M.N., 2006. Ophiolites of the Kamchatsky Mys Peninsula, Eastern Kamchatka: structure, composition, and geodynamic setting. Geotectonics 40, 61–89.

Kinzler, R.J., Grove, T.L., 1992. Primary magmas of mid-ocean ridge basalts. 2. Applications. J. Geophys. Res. 97, 6907–6926.

Lander, A.V., Shapiro, M.N., 2007. The origin of the modern Kamchatka subduction zone. In: Eichelberger, J., Gordeev, E., Kasahara, M., Izbekov, P., Lees, J. (Eds.), Volcanism and Subduction: The Kamchatka Region. American Geophysical Union, Washington, DC, pp. 57–64.

Langmuir, C.H., Klein, E.M., Plank, T., 1992. Petrological systematics of mid-ocean ridge basalts: constraints on melt generation beneath ocean ridges. In: Phipps Morgan, J., Blackman, D.K., Sinton, J.M. (Eds.), Mantle Flow and Melt Generation at Mid-ocean Ridges. AGU, Washington, DC, pp. 183–280.

Maurel, C., Maurel, P., 1982. Etude experimentale de equilibre Fe^{2+}–Fe^{3+} dans les spinelles chromifieres et les liquides silicates basiques coexistants, a 1 atm. C. R. Acad. Sci. (Paris) 295, 209–212.

McKenzie, D., 1985. ^{230}Th–^{238}U disequilibrium and the melting processes beneath ridge axes. Earth Planet. Sci. Lett. 72, 149–157.

Melson, W.G., Byerly, G.R., Nelson, J.A., O'Hearn, T., Wright, T.L., Vallier, T., 1977. A catalogue of the major element geochemistry of abyssal volcanic glasses. Smithson. Contrib. Earth Sci. 19, 31–60.

Pearce, J.A., 2008. Geochemical fingerprinting of oceanic basalts with applications to ophiolite classification and the search for Archean oceanic crust. Lithos 100, 14–48.

Portnyagin, M.V., Magakyan, R., Schmincke, H.-U., 1996. Geochemical variability of boninite magmas: evidence from magmatic inclusions in highly magnesian olivine from lavas of southwestern Cyprus. Petrology 4, 231–246.

Portnyagin, M., Hoernle, K., Avdeiko, G., Hauff, F., Werner, R., Bindeman, I., Uspensky, V., Garbe-Schonberg, D., 2005a. Transition from arc to oceanic magmatism at the Kamchatka–Aleutian junction. Geology 33, 25–28.

Portnyagin, M.V., Savel'ev, D.P., Hoernle, K., 2005b. Plume-related association of cretaceous oceanic basalts of eastern Kamchatka: compositions of spinel and parental magmas. Petrology 13, 571–588.

Portnyagin, M.V., Hoernle, K., Plechov, P.Y., Mironov, N.L., Khubunaya, S.A., 2007. Constraints on mantle melting and composition and nature of slab components in volcanic arcs from volatiles (H_2O, S, Cl, F) and trace elements in melt inclusions from the Kamchatka Arc. Earth Planet. Sci. Lett. 255, 53–69.

Portnyagin, M., Savelyev, D., Hoernle, K., Hauff, F., Garbe-Schönberg, D., 2008. Mid-Cretaceous Hawaiian tholeiites preserved in Kamchatka. Geology 38, 903–906. doi:10.1130/G25171A.1.

Qin, Z., Lu, F., Anderson, J., A.T., 1992. Diffusive reequilibration of melt and fluid inclusions. Am. Miner. 77, 565–576.

Regelous, M., Hofmann, A.W., Abouchami, W., Galer, S.J.G., 2003. Geochemistry of lavas from the Emperor Seamounts, and the geochemical evolution of Hawaiian Magmatism from 85 to 42 Ma. J. Petrol. 44, 113–140.

Riley, G.N., Kolhstedt, D.L., 1991. Melt migration in silicate melt–olivine systems. Earth Planet. Sci. Lett. 105, 500–521.

Rocholl, A.B.E., Simon, K., Jochum, K.P., Molzahn, M., Pernicka, E., Seufert, M., Spettel, B., Stummeier, J., 1997. Chemical characterization of NIST Silicate Glass Certified Reference Material SRM 610 by ICP-MS, TIMS, LIMS, SSMS, INAA, AAS and PIXE. Geostandards 21, 101–114.

Roedder, E., 1984. Fluid inclusions. Miner. Soc. Amer. Book Crafters Inc, Michigan.

Salters, V.J.M., Stracke, A., 2004. Composition of the depleted mantle. Geochem. Geophys. Geosyst. 5, Q05004. doi:10.1029/2003GC000597.

Saveliev, D.P., 2003. Intraplate alkali basalts in the Cretaceous accretionary complex of the Kamchatkan Peninsula (Eastern Kamchatka). Volcanol. Seismol. 1, 14–20 (in Russian).

Shaw, D., 2000. Continuous (dynamic) melting theory revisited. Can. Mineral. 38, 1041–1063.

Shimizu, K., Komiya, T., Hirose, K., Shimizu, N., Maruyama, S., 2001. Cr-spinel, an excellent micro-container for retaining primitive melts — implications for a hydrous plume origin for komatiites. Earth Planet. Sci. Lett. 189, 177–188.

Shimizu, N., 1998. The geochemistry of olivine-hosted melt inclusions in a FAMOUS basalt ALV-519-4-1. Phys. Earth Planet. Inter. 107, 183–201.

Slater, L., McKenzie, D., Gronvold, K., Shimizu, N., 2001. Melt generation and movement beneath Theistareykir, NE Iceland. J. Petrol. 42, 321–354.

Sobolev, A.V., Slutskii, A.B., 1984. Composition and crystallization conditions of the initial melt of the Siberian meimechites in relation to the general problem of ultrabasic magmas. Sov. Geol. Geophys. 25, 93–104.

Sobolev, A.V., Shimizu, N., 1993. Ultra-depleted primary melt included in an olivine from the Mid-Atlantic Ridge. Nature 363, 151–154.

Sobolev, A.V., 1996. Melt inclusions in minerals as a source of principal petrological information. Petrology 4, 209–220.

Sobolev, A.V., Nikogosian, I.K., 1994. Petrology of long-lived mantle plume magmatism: Hawaii, (Pacific) and Reunion Island, (Indian Ocean). Petrology 2, 111–144.

Sobolev, A.V., Hofmann, A.W., Nikogosian, I.K., 2000. Recycled oceanic crust observed in 'ghost plagioclase' within the source of Mauna Loa. Nature 404, 986–990.

Sobolev, A.V., Hofmann, A.W., Sobolev, S.V., Nikogosian, I.K., 2005. An olivine free mantle source of Hawaiian shield basalts. Nature 434, 590–597.

Spandler, C.J., Eggins, S.M., Arculus, R.J., Mavrogenes, J.A., 2000. Using melt inclusions to determine parent-magma compositions of layered intrusions: application to the Greenhills Complex (New Zealand), a platinum group minerals-bearing, island-arc intrusion. Geology 28, 991–994.

Spandler, C., O'Neill, H.S.C., Kamenetsky, V.S., 2007. Survival times of anomalous melt inclusions from element diffusion in olivine and chromite. Nature 447, 303–306.

Spiegelman, M., Kelemen, P.B., 2003. Extreme chemical variability as a consequence of channelized melt transport. Geochem. Geophys. Geosyst. 4 (7).

Sun, S.-S., McDonough, W.F., 1989. Chemical and isotopic systematics of oceanic basalts: implications for mantle composition and processes. In: Saunders, A.D., Norry, M.J. (Eds.), Magmatism in the Ocean Basins. Geological Society Special Publication, London, pp. 313–345.

Wallace, P., Carmichael, I.S.E., 1992. Sulfur in basaltic magmas. Geochim. Cosmochim. Acta 56, 1863–1874.

Workman, R.K., Hart, S.R., 2005. Major and trace element composition of the depleted MORB mantle (DMM). Earth Planet. Sci. Lett. 231, 53–72.

Zlobin, S.K., Kamenetsky, V.S., Sobolev, A.V., Kononkova, N.N., 1990. Initial melt of rocks to complex of the parallel dikes of ophiolites of the Maynitsky zone of Koryakia (study of melt inclusion in chrome spinels). Geokhimiya (11), 1595–1604.